Imaging of cancer cells by multiphoton microscopy using gold nanoparticles and fluorescent dyes

Xiaochao Qu
Xi'an Jiaotong University
The Key Laboratory of Biomedical Information Engineering of the Ministry of Education
Institute of Biomedical Analytical Technology and Instrumentation
School of Life Science and Technology
No. 28 Xianning West Road
Xi'an 710049, China
and
Xidian University
School of Electronic Engineering
Xi'an 710071 China

Jing Wang
Zhenxi Zhang
Xi'an Jiaotong University
The Key Laboratory of Biomedical Information Engineering of the Ministry of Education
Institute of Biomedical Analytical Technology and Instrumentation
School of Life Science and Technology
No. 28 Xianning West Road
Xi'an 710049, China

Norbert Koop
Ramtin Rahmanzadeh
Gereon Hüttmann
University Lübeck
Institute of Biomedical Optics
Peter-Monnik-Weg 4
D-23562 Lübeck, Germany
E-mail: huettmann@bmo.uniluebeck.de

Abstract. Due to their unique optical properties, optical probes, including metal nanoparticles (NPs) and fluorescent dyes, are increasingly used as labeling tools in biological imaging. Using multiphoton microscopy and fluorescence lifetime imaging (FLIM) at 750-nm excitation, we recorded intensity and FLIM images from gold NPs (30 nm) and the fluorescent dye Alexa 488 (A488) conjugated with monoclonal ACT-1 antibodies as well as Hoechst 33258 (H258) after incubation with the lymphoma cell line (Karpas-299). From the FLIM images, we can easily discriminate the imaging difference between cells and optical probes according to their distinct fluorescence lifetimes (cellular autofluorescence: 1 to 2 ns; gold NPs: <0.02 ns; A488: 3.5 ns; H258: 2.5 ns). The NP-ACT-1 and A488-ACT-1 conjugates were bound homogeneously on the surface of cells, whereas H258 stained the cell nucleus. We demonstrate that the emission intensity of gold NPs is about ten times stronger than that of the autofluorescence of Karpas-299 cells at the same excitation power. Compared with fluorescent dyes, stronger emission is also observed from gold NPs. Together with their high photostability, these observations suggest that gold NPs are a viable alternative to fluorescent dyes for cellular imaging and cancer diagnosis. [DOI: 10.1117/1.2942373]

Keywords: multiphoton microscopy; fluorescence lifetime imaging (FLIM); gold nanoparticles (NPs); Alexa Fluor 488; Hoechst 33258; lymphoma cells; Karpas-299.

Paper 07291SSR received Jul. 31, 2007; revised manuscript received Nov. 6, 2007; accepted for publication Nov. 6, 2007; published online Jun. 23, 2008.

1 Introduction

Nowadays, basic biomedical research centers on the investigation of dynamic processes in normal or disease tissues. Optical techniques for cellular imaging are opening new avenues into the exploration of microscopic structures and dynamics for diagnostic application and biological imaging. And these imaging effects will be enhanced when using optical probes as biomarkers.[1,2] Currently used optical probes include fluorescent dyes, noble metal nanoparticles (NPs), quantum dots, etc. Conventional fluorescent dyes have small Stokes shifts, which result in reduced detection sensitivity, and they undergo permanent photobleaching, compromising the ability to view the same region repeatedly or over time. Quantum dots have recently been utilized as fluorescent probes for labeling experiments.[3,4] They can resist photobleaching for a long time, but potential cytotoxicity is the major problem for their application *in vitro* and *in vivo*. Noble metal NPs, in particular, gold, have received widespread interest in their use due to their easy preparation with controlled diameters, ready conjugation with biomolecules, and highly controlled optical properties.[5] Since these nanoparticles do not suffer from photobleaching and phototoxicity,[6] they are considered as attractive alternatives for specific biological labeling.[7,8]

Many previous studies have presented linear optical microscopic techniques, such as fluorescence and confocal scanning microscopy to study cells or tissue, which are unlabeled or labeled by fluorescent dyes and gold NPs.[9,10] Here, we consider, in a different approach, the detection of optical probes by means of nonlinear optical methods. Multiphoton microscopy has gained significant popularity in biomedical imaging in recent years. Using an ultrafast near-infrared laser system, the nonlinear excitation has provided important advantages in its ability to acquire images.[11] Since the multiphoton signal is generated only at the vicinity of the focal spot, where the photon flux is high, the imaging process has enhanced axial depth discrimination and reduced sample photodamage.

In the present work, we used a multiphoton microscope and fluorescence lifetime imaging (FLIM) system to image the lymphoma cell line Karpas-299, which was incubated

Address all correspondence to Gereon Hüttmann, Institute of Biomedical Optics, University Lübeck, Peter-Monnik-Weg 4, D-23562 Lübeck, Germany. Tel: +49–451–500–6530; Fax: +49–451–500–6546; E-mail: huettmann@bmo.uniluebeck.de

1083-3668/2008/13(3)/031217/7/$25.00 © 2008 SPIE

with ACT-1 antibody conjugated gold NPs, ACT-1 conjugated Alexa 488 (A488), and Hoechst 33258 (H258). The optical properties of these optical probes incubated in living cells were compared for different experimental conditions. Our basic study demonstrates that gold NPs, A488, and H258 provide highly efficient emission, which can strengthen cellular imaging. The analysis of fluorescence decay curves within a particular region of interest (ROI) has distinguished different lifetimes between optical probes and cells. It is demonstrated that multiphoton FLIM using gold NPs is a promising technique for biological labeling and imaging.

2 Materials and Methods

2.1 *Multiphoton Imaging System*

The multiphoton imaging system DermaInspect (JenLab, Jena, Germany), which was designed for deep-tissue optical tomography, consisted of a titanium-sapphire laser (Mai Tai, Spectra Physics, Darmstadt, Germany) with 80-MHz pulse frequency, 75-fs pulse duration, and a tuning range of 710 to 920 nm; a scanning module with a motorized shutter; a beam attenuator; and a two-axis galvanometric scanner. A beamsplitter (Chroma 640 DCSPXR, AHF Analysentechnik AG, Tübingen) and a short-pass filter (BG39, Schott, Mainz, Germany) separated the excitation irradiation from the emission. Fluorescence light was detected in the wavelength range between 350 and 600 nm by a photon-counting photomultiplier tube module (PMH 100, Becker & Hickl, Berlin, Germany). High spatial resolution was provided by a high NA oil-immersion objective (Plan-Neofluar 40×, 1.3 oil, Zeiss, Göttingen, Germany) with 140-mm working distance.

The single-photon count rate and the arrival times of the individual photons with respect to the excitation pulse were recorded at each spot in the sample by a PC-based, time-correlated single-photon counting (TCSPC) system (SPC-830, Becker & Hickl, Berlin, Germany).[12] From the measured photon arrival times, fluorescence lifetimes were calculated by a special software (SPCImage, Becker & Hickl, Berlin, Germany), which analyzes and visualizes the fluorescence lifetime data. Curve fitting with a single exponential decay curve to the measured data was used to calculate the fluorescence lifetime for each pixel, which was subsequently displayed in color-coded images.

Evaluation of the fluorescence lifetimes was based either on fitting a single exponential decay curve to the data or by multiexponential fitting with the calculation of a mean decay time.

2.2 *Cell Culture and Sample Preparation*

The human lymphoma cell line Karpas-299 was kindly provided by Research Center Borstel, Borstel, Germany. Cells were routinely grown in suspension culture in RPMI 1640 (1×) medium with hepes and L-glutamine supplemented with 10% fetal calf serum, antibiotic, and antijmycotic solution (all cell culture media, PAA Laboratories, Pasching, Austria) in a 37°C incubator (5% CO_2, 95% air).

Immunogold NPs were made of gold NPs with 30-nm size (British Biocell International, United Kingdom) and ACT-1 antibodies (kindly provided by Professor J. Gerdes, Research Center Borstel, Germany) according to the protocol of the manufacturer. ACT-1 is a monoclonal mouse antibody against CD25, the interleukin-2 receptor (IL-2-R).[13] The fluorescent dye Alexa Fluor 488 (Invitrogen GmbH, Karlsruhe, Germany) was conjugated to the antibodies as recommended by the manufacturer.

Cell suspensions were centrifuged at 1400 rpm for 5 min at 20°C and then resuspended in phosphate-buffered saline (PBS, pH 7.2, containing 1% bovine serum albumin) with cell densities of 10^6 ml^{-1}. Then, either NP-ACT-1 or A488-ACT-1 conjugates was added to the cell suspension at certain ratios between conjugate and cell number. After incubation for 20 min at 37°C, the cells were centrifuged and washed twice and then resuspended in PBS.

Hoechst 33258 (Invitrogen GmbH, Karlsruhe, Germany), which is a fluorescent nucleic acid stain for labeling DNA, was diluted to a concentration of 1 μg/ml with PBS. After the cell suspension was centrifuged and resuspended in PBS, diluted H258 solution was added, and the mixture was incubated for 1 h at 37°C. Then, the cells were centrifuged, and the staining solution was replaced by PBS buffer.

2.3 *Temperature Calculations*

The temperatures inside and surrounding the particles were calculated by an analytical solution of the differential equation of heat diffusion for a single spherical particle that has different thermal properties than the surrounding medium.[14] A series of rectangular 100-fs broad laser pulses with 80-MHz repetition rate was assumed. Since the equations for heat diffusion are linear in time, a superposition of the solutions for a single pulse with appropriate scaling and time delays provided the solution for a pulse train.[15,16] Individual particle absorption was calculated from data that were provided by the manufacturer of the particles for a wavelength of 520 nm (absorption of 5 cm^{-1} at a particle concentration of 7.8×10^{11} ml^{-1}). By absorption measurements with a scanning photometer (Lambda 14, PerkinElmer, Überlingen, Germany) the absorption cross section was scaled to a wavelength of 750 nm. From this calculation, an absorption cross section of 5% of the geometrical cross section was calculated for the 30-nm particles. The focal diameter of the 1.3 NA object was calculated by Abbe's formula[17] to be 700 nm.

3 Results

3.1 *Imaging of Karpas-299 Cells Labeled with NP-ACT-1 Conjugates*

The special linear and nonlinear optical properties of gold NPs have been the subject of recent studies. Multiphoton absorption has been shown to produce strong luminescence of gold NPs.[18] For these experiments, we used gold NPs of two different diameters (15 nm and 30 nm) with the same concentration for multiphoton imaging and compared their luminescence efficiency. Figure 1 shows the intensity images and false-color fluorescence lifetime images of gold NPs with 15-nm (a) and 30-nm (b) diam. A broad range of emission intensities is observed for gold NPs with 15-nm diam in Fig. 1(c). Although it is difficult to quantify their differences precisely due to the range of efficiencies present for gold NPs of the same average size, we observed that gold NPs with 30-nm diam exhibited similar luminescence to 15-nm-diam gold.

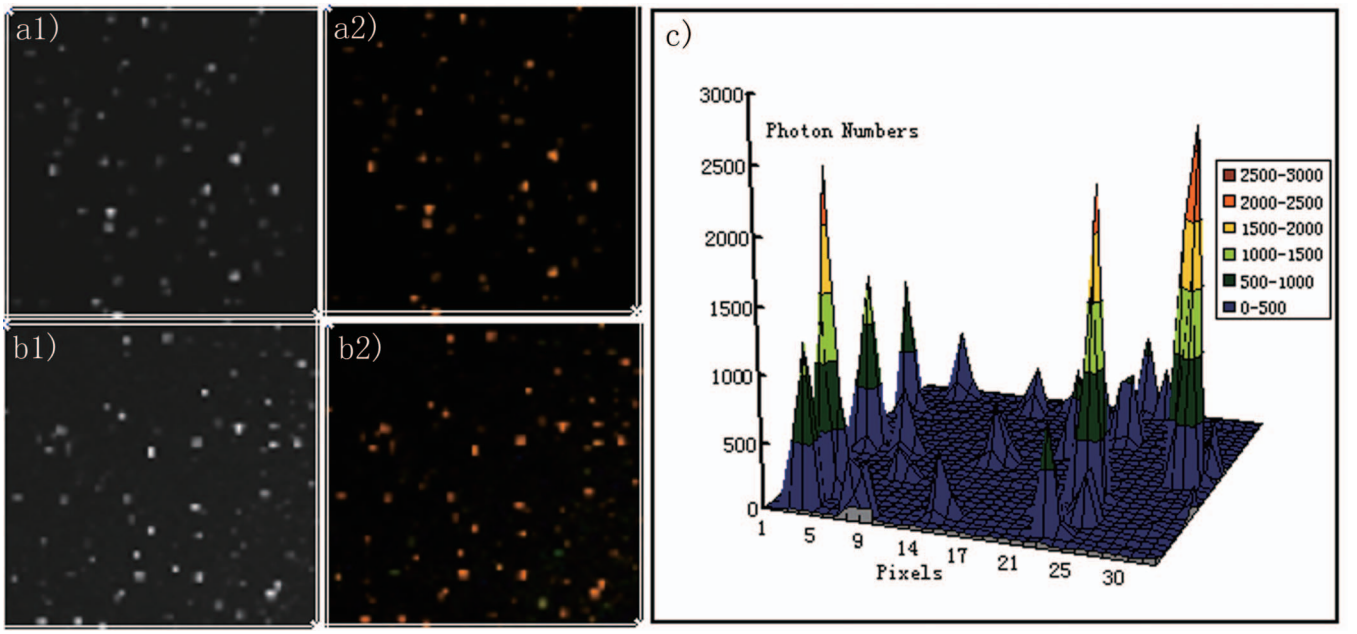

Fig. 1 Intensity images and corresponding false-color FLIM images for gold NPs with different diameters: (a) 15 nm; (b) 30 nm. NP (Excitation wavelength: 750 nm; radiant flux: 20 mW; collection time: 60 s; imaged field: 135 μm). A central region (32×32 pixels) of the image in (a) was represented as contour intensity plot, which is shown in (c).

Only 30-nm-diam gold NPs were chosen for the following cell labeling experiments.

Intensity images and FLIM images of Karpas-299 cells, and cells incubated with NP-ACT-1 conjugates are shown in Fig. 2. According to the different lifetimes of cells and gold NPs, there are some distinct differences between cells incubated without and with gold NPs.

Multiphoton excited fluorescent microscopy of living cells demonstrated individual cellular components at subcellular resolution. An intensity image of the autofluorescent signal

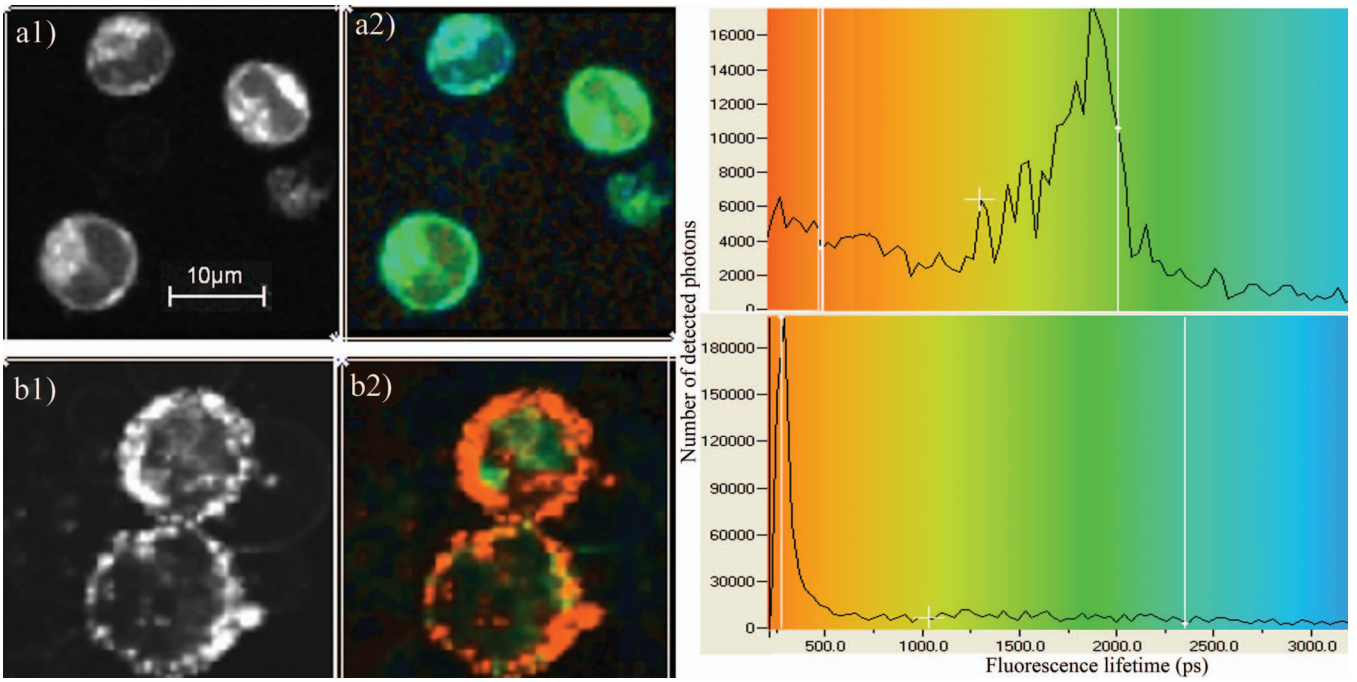

Fig. 2 Intensity images, corresponding false-color FLIM images of Karpas-299 cells (a), and cells incubated with NP-ACT-1 conjugates (b). Excitation wavelength was 750 nm, radiant flux was 20 mW, collection time was 60 s, and imaged field was 90 μm. Histograms of the lifetime distribution of the images are also shown.

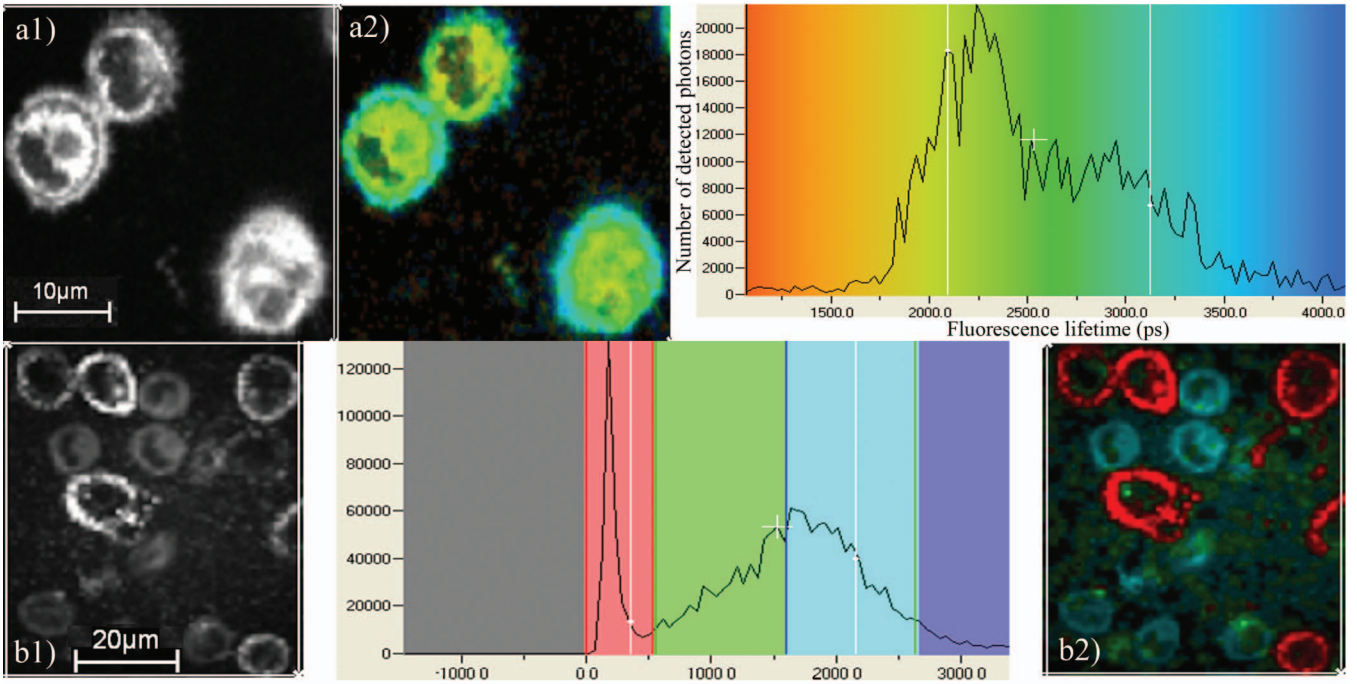

Fig. 3 Intensity image (a1); false-color FLIM image (a2) of Karpas-299 cells incubated with A488-ACT-1 conjugates (excitation wavelength: 750 nm; radiant flux: 25 mW; collection time: 60 s; imaged field: 70 μm); and corresponding histogram of lifetime distribution of the image in (a). (b) Intensity image, discrete false-color FLIM image of cells incubated with A488-ACT-1 and NP-ACT-1 conjugates, and histogram of lifetime distribution in middle column.

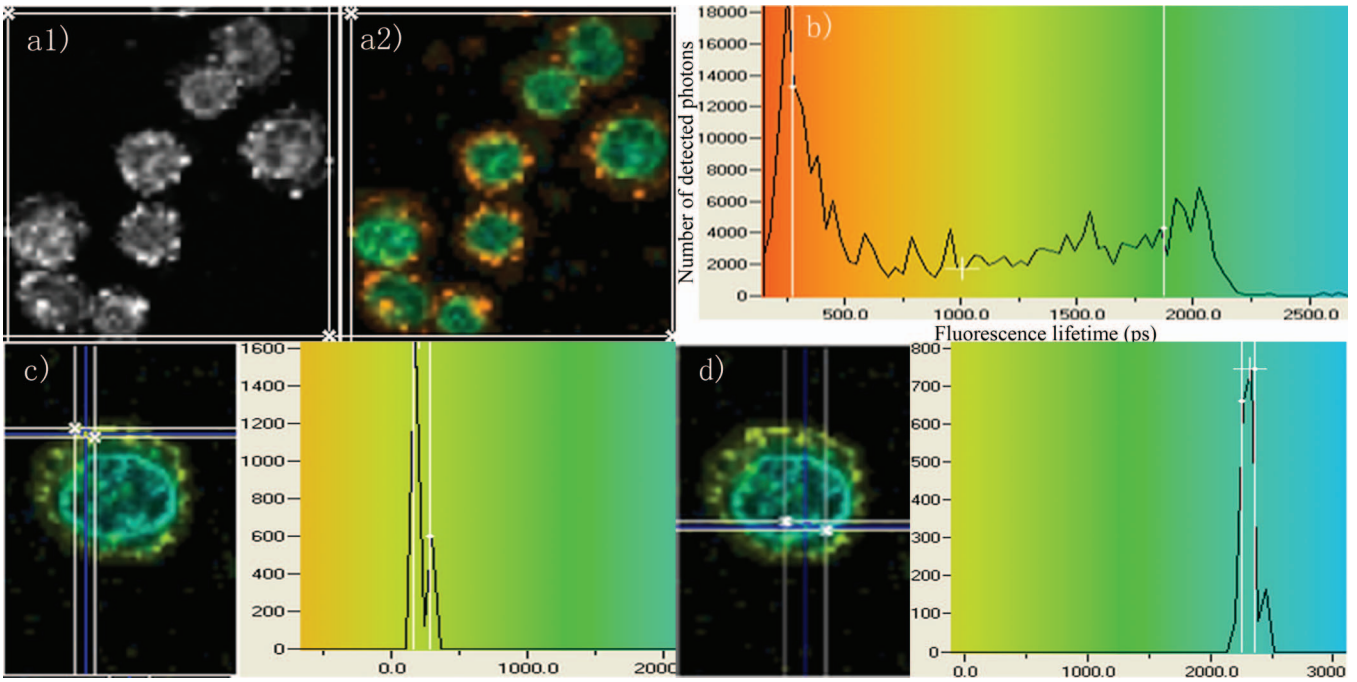

Fig. 4 Multiphoton microscopy of Karpas-299 cells labeled with gold NPs and dyes H258. (a) Intensity image, and corresponding false-color fluorescence lifetime image. (b) Histogram of lifetime distribution of photons within image frame (excitation wavelength: 750 nm, radiant flux: 16 mW; collection time: 60 s). (c) and (d) Analysis for specific area of interest in image delivers the fluorescence lifetime of gold NPs and H258 (imaged field: 90 μm).

delineated cytoplasm and cellular nucleus structure [Fig. 2(a1)]. The corresponding time-resolved fluorescence lifetime measurements demonstrated different lifetimes for different cell compartments [Fig. 2(a2)]. The fluorescence lifetime of Karpas-299 at 750-nm, 20-mW laser excitation measured from the decay curves were 1800 ps for cytoplasmic areas and about 1200 ps for the cellular nucleus.

ACT-1 is a specific antibody to the cell membrane receptor of interleukin-2 (CD25). Due to the binding of ACT-1 to CD25 on the cell surface, gold NPs are only distributed on the surface of cell membrane of Karpas-299 [Fig. 2(b)]. In contrast to the image in Fig. 2(a), binding areas of gold NPs to cell membrane are seen with an additional very short lifetime. Due to the two lifetimes contained in these areas, two or more component fits were needed in these particular areas. For a selected region, the fit curve yields two components with a contribution of 90% of the 195-ps and 10% of an 1800-ps component, which results in a mean fluorescence lifetime of 355 ps. As depicted in the histogram, the fluorescence lifetime of gold NPs is distributed in the red area, whereas the fluorescence lifetime of cellular autofluorescence is typically on the order of 1.0 to 2.0 ns. In fact, the short lifetime of gold NPs was not resolved, because the time resolution was limited by the transit time spread of the detector to about 180 ps.

3.2 *Comparison of Cells Labeled with NP-ACT-1 and A488-ACT-1 Conjugates*

The optical properties of the fluorescent dye A488 were studied through conjugating it to ACT-1 antibodies and incubating Karpas-299 cells with the conjugates. As a relatively new molecular probe, dye A488 is brighter and more resistant to photobleaching than FITC or some other popular dyes.[19]

As expected, the intensity image and false-color FLIM image showed a distinct staining pattern throughout the surface of the cells [Fig. 3(a)]. The corresponding histogram of the lifetime distribution of photons of the image is shown in the right column. The blue color is caused by the dye A488 and corresponds to a mean lifetime of 3.5 ns.

In order to compare the relevant optical properties of gold NPs with fluorescent dye, cell suspension incubated for 20 min with Au-ACT-1 conjugates and A488-ACT-1 conjugates were mixed and prepared as a sample for a direct comparison.

Figure 3(b) shows the intensity image and corresponding discrete false-color FLIM image. According to their different fluorescence lifetimes, gold NPs and A488 can be distinguished easily. Under the same conditions of laser excitation, the emission intensity of gold NPs is much stronger than that of A488. The emission intensity of gold NPs was photostable for hours of continuous irradiation time.

3.3 *Imaging of Cells Labeled with NP-ACT-1 and Dye H258*

As an example for an intracellular stain, we combined gold NPs with the fluorescent probe H258 to characterize their individual optical properties under fluorescence lifetime imaging microscopy. H258 is an important staining molecule for cellular DNA. Prior to the imaging experiment, Karpas-299 cell suspensions were incubated with NP-ACT-1 conjugates and H258.

Figure 4 displays the images obtained from these cells at 750-nm, 15-mW laser excitation. Figure 4(a) shows the intensity image and FLIM image of the sample. A corresponding histogram of the lifetime distribution of the image is shown in Fig. 4(b). When the fluorescence lifetime was analyzed for specific areas of interest, a long lifetime was found in the nuclear area that was stained by H258 (d), and a short one was found in the membrane area labeled by gold NPs (c). The blue-green color shows regions stained with H258 with lifetime of 2.5 ns, which is comparable to that found in spectroscopic time-resolved measurements,[20] the yellow color shows gold NPs.

3.4 *Cell Damage*

Under laser irradiation of NP-ACT-1 incubated cell with more than 20 mW cell damage with bleb formation was observed.[21] In contrast to a fluorescent dye, gold NPs have a high-absorption cross section and a low-fluorescence quantum yield. Additionally, there is still a few percent residual linear absorption at 750 nm. Temperature calculations show that this leads to a significant temperature increase inside the particles of 30 K/mW irradiation power at the end of each pulse [Fig. 5(a)]. Under conditions of cell damage, with an average radiant flux above 20 mW, the temperature increase is larger than 600 K. However, at the beginning of the next pulse, which follows after 12 ns, the temperature is cooled down below 2 K. Within 100 ns, an average background temperature of 15 K is established, on which 600-K particle heating of the individual laser pulses occurs. The temperature increase is highly confined to the particle. At the end of the first femtosecond laser pulse, the temperature increase outside of the particle is virtually zero [Fig. 5(b)]. Even after a steady state is established, the elevated temperature is still confined to a few tens of nanometers.

4 Conclusion

Multiphoton excitation microscopy provides attractive advantages over conventional one-photon imaging microscopy and can be employed as novel noncontact biomedical tools for three-dimensional (3-D) resolved fluorescence imaging and optical diagnostics.[22–24] Because multiphoton excitation at high intensities occurs only in the minute focal volume of a high numerical aperture objective, photobleaching and photodamage are minimized to the focal region.[25] FLIM offers powerful tools for the discrimination of different fluorescent species.

These preliminary experiments show clearly that high resolution, intensity, and fluorescence lifetime images of cancer cells incubated with three different optical probes are possible by multiphoton imaging. On the basis of the different fluorescence lifetimes of these optical probes, we can easily discriminate them when imaging under different experimental conditions. Due to the specific binding of ACT-1 to the membrane receptor CD25, NP-ACT-1 conjugates and A488-ACT-1 conjugates stained homogeneously and specifically only the surface of cell membranes of Karpas-299. Under the same conditions with 750-nm, 20-mW laser excitation, the emission intensity of gold NPs is stronger than the autofluorescence of

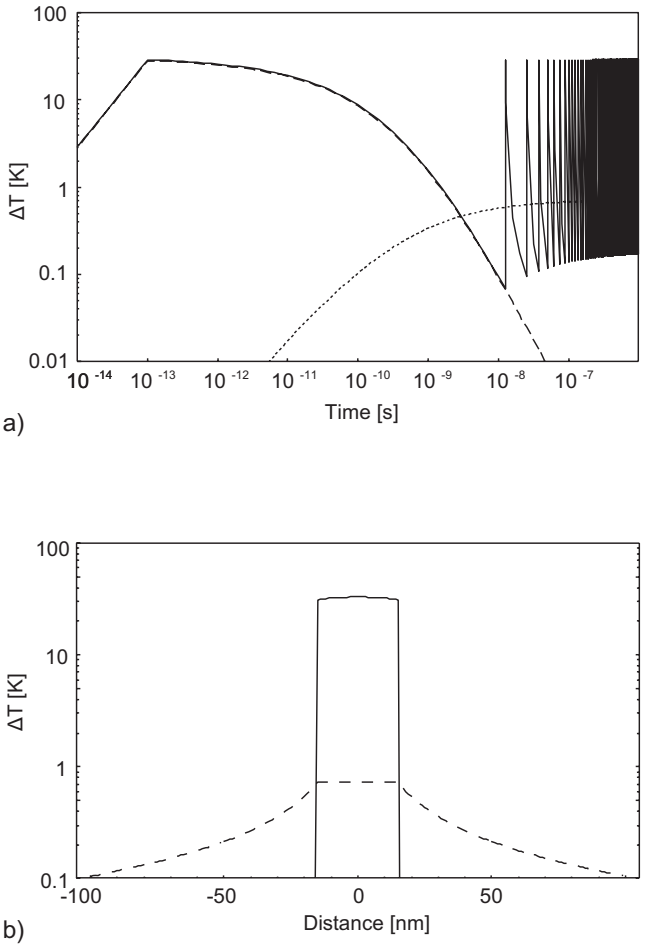

Fig. 5 Calculation of the temperature in and around single gold particles during laser irradiation. (a) Temperature course inside a 30–nm NP during the irradiation with 1-mW radiant flux focused to a spot of 700 nm (solid black line). Rectangular pulses with 100-fs width and 12-nm temporal separation were assumed. Additionally, the temperature course after one pulse (dashed line) and after true CW irradiation with the same average radiant flux (dotted line) are shown (b) Spatial temperature distribution at the end of the first pulse (solid line) and after 10 μs irradiation (dashed line).

the cells. Compared to commonly used fluorescent dyes, gold NPs showed comparable or higher fluorescence intensity and good photostability.

Modern systems can resolve the decay curve to enable multiexponential fitting. Several decay components caused by autofluorescence, fluorescent dyes, and gold NPs can be distinguished. With the development of practical time-gated detection schemes, multiphoton FLIM may in future also be used for clinical applications.

Slightly above the radiant flux of 20 mW, which was needed for autofluorescence imaging, cell damage by the gold conjugates was observed.[21] A destruction of cells by laser-irradiated gold NPs was described for different laser parameters.[26–31] Under pulsed irradiation, microbubbles may directly destroy the cell membrane, whereas a continuous irradiation locally heats the cells above a certain damage threshold.

Temperature calculations reveal that in contrast to fluorescent dye molecules, significant heating of the particles is expected at imaging conditions. Two heating phases were distinguished. A high temperature increase of several hundred Kelvin inside the particle, which rapidly cooled down to nearly the base temperature between two pulses and does not affect the surroundings, and an increase of the background temperature by a few tens of Kelvin after a few hundred nanoseconds of imaging. The background temperature spreads only a few tens of nanometers away from the particle surface.

For single gold particles, under our irradiation conditions, the average temperature increase is not high enough for cell destruction, but the peak particle temperature at the end of the pulse may lead to vaporization of water and bubble formation. When the cell membrane is stained with a large number of gold NPs, an overlap of the temperature profiles of individual particles may further significantly increase the background temperature. Therefore, the damage threshold and mechanism are expected to depend not only on particles and irradiation parameters but also on the labeling density of the cells.

In summary, this study demonstrates cellular imaging with improved contrast based on gold NPs in addition to conventional fluorescent dyes, when near-infrared multiphoton excitation laser scanning microscopy is used. Gold NPs are easily bioconjugated, and their special optical properties are unique in comparison with other optical probes. Future experiments will address gold conjugates with new antibody for imaging different kinds of cells and a study on the extent of photodamage and the photothermolysis to normal cells and diseased cells.

Acknowledgments

We thank the Research Center Borstel for supplying the Karpas-299 cell line and for their help during the preparation of immunooptical probes and samples. We acknowledge Barbara Flucke, Margit Kernbach, Bever Marco, and Astrid Rodewald of the Institute of Biomedical Optics and Cuiping Yao of the School of Life Science and Technology for their assistance during these experiments. This study was supported by the National Nature Science Foundation of China (Grant No. 60578026) and the Project-Based Personnel Exchange Programme with CSC and DAAD (2006).

References

1. S. Weiss, "Fluorescence spectroscopy of single biomolecules," *Science* **283**(5408), 1676–1683 (1999).
2. P. Alivisatos, "The use of nanocrystals in biological detection," *Nat. Biotechnol.* **22**(1), 47–52 (2004).
3. X. Y. Wu, H. J. Liu, J. Q. Liu, K. N. Haley, J. A. Treadway, J. P. Larson, N. F. Ge, F. Peale, and M. P. Bruchez, "Immunofluorescent labeling of cancer marker Her2 and other cellular targets with semiconductor quantum dots," *Nat. Biotechnol.* **21**(1), 41–46 (2003).
4. X. Michalet, F. F. Pinaud, L. A. Bentolila, J. M. Tsay, S. Doose, J. J. Li, G. Sundaresan, A. M. Wu, S. S. Gambhir, and S. Weiss, "Quantum dots for live cells, *in vivo* imaging, and diagnostics," *Science* **307**(5709), 538–544 (2005).
5. J. L. West and N. J. Halas, "Applications of nanotechnology to biotechnology—commentary," *Curr. Opin. Biotechnol.* **11**(2), 215–217 (2000).
6. J. Yguerabide and E. E. Yguerabide, "Light-scattering submicroscopic particles as highly fluorescent analogs and their use as tracer labels in clinical and biological applications—I. theory," *Anal. Biochem.* **262**(2), 137–156 (1998).
7. A. Shamsaie, M. Jonczyk, J. Sturgis, J. P. Robinson, and J. Irudayaraj, "Intracellularly grown gold nanoparticles as potential surface-enhanced Raman scattering probes," *J. Biomed. Opt.* **12**(2), 020502 (2007).

8. P. J. Campagnola, H. A. Clark, W. A. Mohler, A. Lewis, and L. M. Loew, "Second-harmonic imaging microscopy of living cells," *J. Biomed. Opt.* **6**(3), 277–286 (2001).
9. S. G. Megason and S. E. Fraser, "Imaging in systems biology," *Cell* **130**(5), 784–795 (2007).
10. I. H. El-Sayed, X. H. Huang, and M. A. El-Sayed, "Surface plasmon resonance scattering and absorption of anti-EGFR antibody conjugated gold nanoparticles in cancer diagnostics: applications in oral cancer," *Nano Lett.* **5**(5), 829–834 (2005).
11. P. T. C. So, C. Y. Dong, B. R. Masters, and K. M. Berland, "Two-photon excitation fluorescence microscopy," *Annu. Rev. Biomed. Eng.* **2**, 399–429 (2000).
12. W. A. Becker, A. Bergmann, K. Koenig, and U. Tirlapur, "Picosecond fluorescence lifetime microscopy by TCSP imaging," *Proc. SPIE* **4262**, 414–419 (2001).
13. R. Schwarting, J. Gerdes, A. Ziegler, and H. Stein, "Immunoprecipitation of the interleukin-2 receptor from Hodgkin's disease derived cell lines by monoclonal antibodies," *Hematol. Oncol.* **5**, 57–64 (1987).
14. H. Goldenberg and C. J. Tranter, "Heat flow in an infinite medium heated by a sphere," *Br. J. Appl. Phys.* **3**, 296–298 (1952).
15. G. Hüttmann, J. Serbin, B. Radt, B. I. Lange, and R. Birngruber, "Model system for investigating laser-induced subcellular microeffects," *Proc. SPIE* **4257**, 398–409 (2001).
16. R. Roider and R. Birngruber, "Solution of the heat conduction equation," in *Optical-Thermal Response of Laser-Irradiated Tissue*, A. J. Welch, M. J. C. van Gemert, Eds., pp. 385–409, Plenum Press, New York (1995).
17. A. Vogel, J. Noack, G. Hüttmann, and G. Paltauf, "Mechanisms of femtosecond laser nanosurgery of cells and tissues," *Appl. Phys. B* **81**, 1015–1047 (2005).
18. R. A. Farrer, F. L. Butterfield, V. W. Chen, and J. T. Fourkas, "Highly efficient multiphoton-absorption-induced luminescence from gold nanoparticles," *Nano Lett.* **5**(6), 1139–1142 (2005).
19. N. Panchuk-Voloshina, R. P. Haugland, J. Bishop-Stewart, M. K. Bhalgat, P. J. Millard, F. Mao, W. Y. Leung, and R. P. Haugland, "Alexa dyes, a series of new fluorescent dyes that yield exceptionally bright, photostable conjugates," *J. Histochem. Cytochem.* **47**(9), 1179–1188 (1999).
20. B. L. Sailer, A. J. Nastasi, J. G. Valdez, J. A. Steinkamp, and H. A. Crissman, "Differential effects of deuterium oxide on the fluorescence lifetimes and intensities of dyes with different modes of binding to DNA," *J. Histochem. Cytochem.* **45**(2), 165–175 (1997).
21. X. C. Qu, N. Koop, Z. Li, J. Wang, Z. X. Zhang, and G. Hüttmann, "Multiphoton fluorescence lifetime imaging of Karpas-299 cells using ACT-1 antibody conjugated gold nanoparticles," *Proc. SPIE* **6630**, 66301C (2007).
22. T. Gura, "Multiphoton imaging—biologists get up close and personal with live cells," *Science* **276**(5321), 1988–1990 (1997).
23. S. Kantelhardt, J. Leppert, N. Petkus, G. Hüttmann, V. Rohde, and A. Giese, "Multiphoton microscopy and fluorescence lifetime imaging of brain and brain tumor tissue," *J. Neuro-Oncol.* **8**(4), 494–494 (2006).
24. J. Leppert, J. Krajewski, S. R. Kantelhardt, S. Schlaffer, N. Petkus, E. Reusche, G. Hüttmann, and A. Giese, "Multiphoton excitation of autofluorescence for microscopy of glioma tissue," *Neurosurgery* **58**(4), 759–767 (2006).
25. K. König, "Multiphoton microscopy in life sciences," *J. Microsc.* **200**, 83–104 (2000).
26. J. Y. Chen, D. L. Wang, J. F. Xi, L. Au, A. Siekkinen, A. Warsen, and X. D. Li, "Immuno gold nanocages with tailored optical properties for targeted photothermal destruction of cancer cells," *Nano Lett.* **7**(5), 1318–4322 (2007).
27. C. P. Yao, R. Rahmanzadeh, E. Endl, Z. X. Zhang, J. Gerdes, and G. Hüttmann, "Elevation of plasma membrane permeability by laser irradiation of selectively bound nanoparticles," *J. Biomed. Opt.* **10**(6), 064012 (2005).
28. I. H. El-Sayed, X. H. Huang, and M. A. El-Sayed, "Selective laser photo-thermal therapy of epithelial carcinoma using anti-EGFR antibody conjugated gold nanoparticles," *Cancer Lett.* **239**(1), 129–135 (2006).
29. C. Loo, A. Lowery, N. Halas, J. West, and R. Drezek, "Immunotargeted nanoshells for integrated cancer imaging and therapy," *Nano Lett.* **5**(4), 709–711 (2005).
30. C. M. Pitsillides, E. K. Joe, X. B. Wei, R. R. Anderson, and C. P. Lin, "Selective cell targeting with light-absorbing microparticles and nanoparticles," *Biophys. J.* **84**(6), 4023–4032 (2003).
31. G. Hüttmann and R. Birngruber, "On the possibility of high-precision photo-thermal microeffects and the measurement of fast thermal denaturation of proteins," *IEEE J. Sel. Top. Quantum Electron.* **5**(4), 954–962 (1999).